Refilling of the slot region between the inner and outer electron radiation belts during geomagnetic storms

R. M. Thorne,[1] Y. Y. Shprits,[1] N. P. Meredith,[2] R. B. Horne,[2] W.Li,[1] and L. R. Lyons[1]

R. B. Horne and N. P. Meredith, British Antarctic Survey, Natural Environment Research Council, Madingley Road, Cambridge, CB3 0ET, UK. (r.horne@bas.ac.uk; nmer@bas.ac.uk)

W. Li, L. R. Lyons, Y. Y. Shprits, and R. M. Thorne, Department of Atmospheric and Oceanic Sciences, University of California, Los Angeles, 405 Hilgard Avenue, Los Angeles, CA 90095-1565, USA. (moonli@atmos.ucla.edu; larry@atmos.ucla.edu; yshprits@atmos.ucla.edu; rmt@atmos.ucla.edu)

[1]Department of Atmospheric and Oceanic Sciences, University of California, Los Angeles, USA.

[2]British Antarctic Survey, Natural Environment Research Council, Cambridge, UK.

Abstract. Energetic electrons ($\geq$ 50 keV) are injected into the slot region ($2 < L < 4$) between the inner and outer radiation belts during the early recovery phase of geomagnetic storms. Enhanced convection from the plasmasheet can account for the storm-time injection at lower energies, but does not explain the rapid appearance of higher energy electrons ($\geq$ 150 keV). The effectiveness of either radial diffusion (driven by enhanced ULF waves) or local acceleration (during interactions with enhanced whistler-mode chorus emissions), as a potential source for refilling the slot at higher energies, is analyzed for observed conditions during the early recovery phase of the October 10, 1990 storm. We demonstrate that local acceleration, driven by observed chorus emissions, can account for the rapid enhancement in 200-700 keV electrons in the outer slot region near $L = 3.3$. Radial diffusion is much less effective, but may partially contribute to the flux enhancement at lower L. Subsequent outward expansion of the plasmapause during the storm recovery phase effectively terminates local wave acceleration in the slot, and prevents acceleration to energies higher than $\sim$ 700 keV. A statistical analysis of energetic electron flux enhancements and wave and plasma properties over the entire CRRES mission supports the concept of local wave acceleration as a dominant process for refilling the slot during the main and early recovery phase of storms. For moderate storms, the injection process naturally becomes less effective at energies $\geq$ 1 MeV, due to the longer wave acceleration times and additional precipitation loss from scattering by EMIC waves. However, during extreme events when the plasmapause remains com-

pressed for several days, conditions may occur to allow wave acceleration to multi-MeV energies at locations normally associated with the slot.

1. Introduction

Energetic electrons ($\geq$ 150 keV) in the Earth's radiation belts are distributed in two distinct regions. The inner belt (1.2-2 R_E) is relatively stable and usually exhibits only minor variability to solar-induced disturbances. In contrast, the outer belt ($> 4R_E$) is highly variable, with flux changes exceeding an order of magnitude over periods as short as an hour. Under quiet geomagnetic conditions, a pronounced "slot" or gap forms between the two belts (orbit 182 in the lower panel of Figure 1). The quiet-time slot is most pronounced at energies above several hundred keV. The basic structure of the slot has been explained as a balance between slow inward radial diffusion from a source population in the outer zone and precipitation losses from the inner magnetosphere, primarily due to resonant scattering by plasmaspheric hiss [*Lyons and Thorne*, 1973] and other whistler-mode waves [*Abel and Thorne*, 1998a,b]. Owing to the long time-scales associated with radial diffusion in the inner magnetosphere, only electrons with energies below the minimum energy for resonance with whistler-mode waves (or magnetic moments $\mu = {p_\perp}^2/2mB < 10$ Mev/G) are able to diffuse into the inner zone without substantial loss.

During a geomagnetic storm, the flux of energetic electrons in the outer radiation zone and the slot region can be substantially enhanced. Flux changes during the October 10, 1990 geomagnetic storm are shown in Figure 1. Pre-storm conditions (orbit 182) exhibit a well-defined two-zone structure, with energetic (E $\geq$ 340 keV) electron flux drops exceeding 3 orders of magnitude in the center of the slot, $2.7 \leq L \leq 3.5$. The Combined Release and Radiation Effects Satellite (CRRES) was ideally located to monitor changes in the radiation belts, and some of the important physical processes responsible

for variability in the outer zone ($L \geq 4$) during this storm have been explored in previous studies [e.g., *Brautigam and Albert*, 2000; *Meredith et al.*, 2002a,b; *Summers et al.*, 2002; *Horne et al.*, 2003b; *Liu et al.*, 2003; *Iles et al.*, 2006]. We concentrate here on the processes responsible for the rapid filling of the slot region ($L \sim 3$) at energies above a few hundred keV, over a period of less than 9.5 hours, between the main phase of the storm (orbit 186) and the early recovery phase (orbit 187). Lower energy electrons (153 keV channel) are rapidly injected into the slot region and outer belt during the main phase of the storm, and remain at enhanced levels throughout the entire storm recovery. In contrast, higher energy electrons (340 and 510 keV channels) are slightly depleted (near $L = 3$) during the main phase (orbit 186), but rapidly recover to levels well above the pre-storm values in the early recovery (orbit 187). The relative flux increase is most pronounced near the center of the quite-time slot. Interestingly, there is no evidence for a flux increase at this location at energies above 1 MeV, although such relativistic electrons do show substantial increase in the outer radiation zone over the extended recovery phase of the storm, as described by *Meredith et al.* [2002a]. Here we investigate the effectiveness of three potential mechanisms to account for the rapid electron flux increases in the slot region, normally devoid of energetic electrons. A statistical analysis of slot region filling for storm-time conditions during the entire CRRES mission is also presented. The statistical analysis supports the general applicability of our case study, and we conclude with a discussion of the dominant physical process responsible for electron variability in the slot region.

2. Convective Transport from the Plasmasheet

The main phase of a magnetic storm is characterized by the development of an enhanced and sustained convection electric field, which carries plasmasheet ions and electrons into the inner magnetosphere (leading to the formation of the storm-time ring current [e.g., *Daglis et al.*, 1999]), and also leads to a redistribution of thermal plasma in the inner magnetosphere, specifically erosion and compression of the nightside plasmasphere and the development of a dayside plume [*Goldstein et al.*, 2005]. Under purely adiabatic transport, conservation of the first adiabatic invariant (μ) and total energy (μB + qΦ) requires that plasmasheet particles gain kinetic energy as they are injected into regions of stronger magnetic field. Particle kinetic energy gain comes at the expense of a drop in electrostatic potential energy, which is limited by the strength of the convection electric field imposed across the magnetosphere. *Liu et al.* [2003] have simulated the convective injection of plasmasheet electrons into the inner magnetosphere, using a realistic model for the storm-time electric field. Their simulations adequately account for the observed injection of ring current electrons at energies below 150 keV during the October 1990 storm, but they were unable to explain the injection of higher energy electrons into the region $3 \leq L \leq 5$. This difference is primarily due to the large gradient drift of higher energy electrons, which prevents them from penetrating into the region inside $L \sim 5$. Figure 2 shows the drift paths of electrons with $\mu = 3$ and 30 MeV/G in a dipole magnetic field and a Volland-Stern electric field [*Volland*, 1973; *Stern*, 1975] under both quiet (left panels, $\Delta\Phi = 25$ kV) and storm-time (right panels, $\Delta\Phi = 200$ kV) conditions, where $\Delta\Phi$ is the total potential drop across the magnetosphere. The storm-time enhancement of the convection electric field allows thermal (3 MeV/G) plasmasheet electrons to penetrate

into $L \approx 3$ near dawn. During the inward transport, the electron energy rises from ~ 1 keV at $L = 10$ to typical ring current energies ~ 30 keV at $L = 3$. In contrast, higher energy (30 MeV/G) plasmasheet electrons are only able to penetrate to $L \sim 5$, where their energies are ~ 70 keV. Modeling by *Liu et al.* [2003], using realistic fluctuations of the convection electric field during the main phase of the October 1990 storm, indicates that additional radial diffusive transport also occurs, but only electrons below 150 keV are able to be injected into the region between $3 \leq L \leq 5$. The rapid enhancement in 300-500 keV electron flux must therefore be due to a different process.

3. Inward Radial Diffusion

Enhanced ULF wave activity during magnetic storms [*Mathie and Mann*, 2000] can cause inward radial diffusion and an associated increase in energetic electron flux [*Elkington et al.*, 2003; *Shprits et al.*, 2005]. Temporal changes in energetic electron phase space density f can be modeled using the radial diffusion equation [*Schulz and Lanzerotti*, 1974]

$$\frac{\partial f}{\partial t} = L^2 \frac{\partial}{\partial L}\left(\frac{D_{LL}}{L^2}\frac{\partial f}{\partial L}\right) - \frac{f}{\tau}, \tag{1}$$

where the first term on the right is due to radial diffusion and the second term represents losses. D_{LL} is the radial diffusion coefficient and τ is the loss time-scale. The radial profile of phase space density is controlled by the competition between diffusive transport and loss [*Thorne*, 1982]. The diffusion coefficient D_{LL} is usually represented as a sum of coefficients for magnetic D_{LL}^M and electrostatic D_{LL}^E field fluctuations. An empirical scaling of D_{LL}, for different levels of the geomagnetic activity index Kp, has been obtained from satellite data and shows that $D_{LL}^M > D_{LL}^E$ for $L \geq 3$ [*Brautigam and Albert*, 2000]. For

$1 \leq Kp \leq 6$, the magnetic diffusion coefficient can be expressed as

$$D_{LL}^{M} = 10^{(0.506Kp-9.325)} L^{10} day^{-1}. \quad (2)$$

Although the rate of radial diffusion becomes much weaker at smaller L, enhanced ULF wave activity during the main phase of a storm and strong gradients in phase space density inside $L \sim 4$ could still facilitate the transport of energetic outer zone electrons into lower L [e.g., *Shprits and Thorne*, 2004]. To investigate the effectiveness of this process, we have performed a time-dependent simulation of anticipated inward diffusion over a 10 hour period (between CRRES orbits 186 and 187), during the early recovery phase of the October 1990 storm. Since measured flux at higher L shells varies significantly during the main phase due to adiabatic effects [*Kim and Chan*, 1997], we chose to start our simulation with a steady state profile computed for conditions with Kp = 6 and $\tau = 1$ day. The radial flux profile obtained (solid line in Figure 3) gives an adequate fit to the observed flux at 340 keV at higher L shells (on orbit 187) and mimics the pronounced drop observed on orbit 186 in the region $L < 4$, where adiabatic effects become negligible. This starting condition provides a liberal estimate of the source population for subsequent inward radial diffusion. Throughout the simulation we adopt an inner boundary condition $f = 0$ at $L = 1$. The outer boundary condition (at L=7) is modeled by an exponential fit to the average flux measured on CRRES:

$$J(K, L = 7) = 8222.6exp(-7.068K) cm^{-2} sr^{-1} keV^{-1} s^{-1}, \quad (3)$$

where K is the kinetic energy in MeV. The rate of radial diffusion is computed using expression (2) and measured Kp values. Particle lifetimes are assumed to be 100 days. Following *Shprits et al.* [2005], we solve for the normalized phase space density $f(L)$

at a fixed magnetic moment, and use the boundary condition (3) to obtain differential flux $J(K, L)$ at a fixed kinetic energy. The modeled electron flux at 340 keV is shown at intervals of five (dash dot) and 10 (dashed) hours into the simulation. Even with this conservative loss-free assumption, inward radial diffusion is unable to account for the dramatic flux increase in high energy electron flux observed throughout the slot region between CRRES orbits 186 (storm main phase) and 187 (early recovery). However, electrons present near the inner edge of the outer zone can be transported inward by about 0.3 R_E over a 10 hour interval. This conclusion is relatively insensitive to the adopted lifetime parameter (unless $\tau \leq 10$ hours).

4. Local Acceleration During Interactions with Chorus Emission

The time history of geomagnetic activity (AE and Kp in the upper panels of Figure 1) indicates that sustained but impulsive convection occurred throughout the recovery phase of the storm [*Meredith et al.*, 2002a]. This convection led to the episodic injection of thermal plasmasheet electrons into the low density region outside the storm-time plasmapause. During the main (and early recovery) phase of the storm, the plasmapause was eroded and compressed well inside L=3, and strong whistler-mode chorus emissions were observed in the low-density region exterior to the dawn-side plasmapause (top panel of Figure 1). Whistler-mode chorus can interact with electrons over a broad energy range, leading to scattering in both pitch-angle and energy [*Horne and Thorne*, 1998; *Summers et al.*, 1998]. Enhanced inward convection (section 2) provides a seed population of 10 keV to $\sim$ 100 keV electrons throughout the region exterior to the storm-time plasmapause. Conservation of the first two adiabatic invariants leads to anisotropic electron distributions with $T_\perp > T_\parallel$ (where $T_\perp$ and $T_\parallel$ are temperatures perpendicular and parallel to the

ambient magnetic field, respectively) during inward transport. The anisotropic electron distributions provide the source of free energy for the excitation of whistler-mode chorus waves at frequencies below the electron gyrofrequency [e.g., *Horne et al.*, 2003c]. Waves grow by scattering particles into the loss cone at small pitch-angles [*Kennel and Petschek*, 1966], but they also scatter electrons to higher energies at large pitch-angles [*Horne and Thorne*, 2003]. The net result is a local transfer of energy between the injected ring current (10-100 keV) electrons and relativistic electrons using chorus waves as an intermediary. This local acceleration is most effective in regions where the ratio of the electron plasma frequency to the cyclotron frequency (f_{pe}/f_{ce}) is small, typically less than 4 [*Horne et al.*, 2003a, 2005a]. Low values of f_{pe}/f_{ce} increase the phase velocity of the waves and enable more effective energy diffusion in locations just outside the plasmapause. Energy diffusion, leading to a hardening of the electron energy spectrum, should continue as long as chorus waves are excited and the ratio of f_{pe}/f_{ce} remains low. Recent studies have shown that local acceleration by chorus emissions can account for the gradual buildup of outer zone relativistic electron flux over a period comparable to a few days in the recovery phase of storms [*Summers et al.*, 2002; *Horne et al.*, 2005a,b; *Thorne et al.*. 2005a; *Shprits et al.*, 2006a]. The local wave acceleration process can be distinguished from inward radial diffusion, since it naturally leads to a gradual build-up of localized peaks in phase space density [*Green and Kivelson*, 2004; *Iles et al.*, 2006].

Local acceleration by chorus emissions should also have been effective in the slot region (near L=3), during the early recovery phase of the October 1990 storm, since the plasmapause remained compressed inside this location and intense chorus emissions were observed in the region exterior to $L \sim 2.7$ (top panel of Figure 1 and lower panel of

Figure 4). The CRRES observations on orbit 186 were taken at relatively high latitude, well away from the expected wave excitation region near the equator. Ray tracing studies show that waves excited with field-aligned propagation vectors tend to migrate outwards to slightly higher L during propagation to higher latitude [*Horne and Thorne*, 2003]. To account for this cross field propagation we average over a narrow range of L values, to obtain an estimate of the power spectral intensity of chorus emissions at various locations in the slot region.

Chorus emissions are typically observed over a broad MLT range (2300-1400), with an intensity primarily controlled by the level of geomagnetic activity [*Meredith et al.*, 2001]. A statistical analysis of chorus emissions during storm conditions [*Meredith et al.*, 2003a] indicates that the most intense waves in the midnight sector ($\sim$ 2400 MLT) are confined to latitudes within $10 \sim 15$ degrees of the equator, while chorus in the post dawn quadrant (0600-1200 MLT) extends to much higher latitudes ($\geq 30^o$). During the main and early recovery phase of the October storm the geomagnetic activity index remained high (Kp ≥ 5), and the variation in chorus intensity illustrated in the top panel of Figure 1 is primarily associated with changes in the magnetic latitude and MLT during successive passes of the CRRES spacecraft through the magnetosphere. All outbound passes through the slot region ($2.5 \leq L \leq 4.0$) occurred near midnight, while the inbound passes occurred in the post-dawn sector [*Meredith et al.*, 2002b]. Furthermore, the night side outbound pass during orbit 186 was made at a latitude ($\lambda_m \geq 15^\circ$) where chorus is subject to severe Landau damping [*Bortnik et al.*, 2007], consistent with the observed statistical distribution [*Meredith et al.*, 2003a]. In contrast, measurements of chorus on the inbound dayside pass (on orbit 186) were made at a latitude near $21 - 22^\circ$, where

chorus emissions are expected to be most intense [*Meredith et al.*, 2003a]. Consequently, in the modeling described below, we assume that the local measurements of chorus power spectral intensity obtained on the inbound dayside pass (orbit 186) are representative of emissions over the entire dawn-side during the period of electron acceleration in the early recovery phase of the storm.

The spectral intensity of lower band chorus emissions, observed on the inbound orbit 186 of CRRES at locations $3.35 \geq L \leq 3.55$ are shown in the middle panel of Figure 4 as a function of wave frequency normalized to the equatorial gyro-frequency f_{ce} . A least squares Gaussian fit (red), with $B_w = 46.2\ pT$, peak frequency $f_m = 0.29 f_{ce}$, and bandwidth $\delta f = 0.11 f_{ce}$ was obtained to the average spectral intensity of chorus in the outer slot (green). Corresponding fits to the spectral intensity for $3.05 \geq L \leq 3.25$ are shown in the top panel. The trough density model of *Sheeley et al.* [2001], and a dipole magnetic field was used to estimate the ratio of f_{pe}/f_{ce} at the equator, and the density was assumed to be constant with latitude. Electron scattering is assumed to occur over a latitude range $-15^o < \lambda_m < 15^o$ between 2400-0600 MLT and over a range $-35^o < \lambda_m < 35^o$ between 0600-1200 MLT. Gaussian fits to the spectra observed on the dayside (Figure 4), together with the adopted latitudinal distributions, were then used to computed the bounce and drift-averaged rates of pitch-angle $\langle D_{\alpha\alpha} \rangle$ and momentum diffusion $\langle D_{pp} \rangle$ at $L = 3.35$ (Figure 5) and $L = 3.05$ (not shown), using a simplified quasi-linear code developed at UCLA [*Shprits et al.*, 2006b]. Since the bounce-averaged pitch-angle and energy diffusion coefficients, obtained under the simplifying assumption of field-aligned propagation, agree well [*Shprits et al.*, 2006b] with exact calculations with the PADIE code [*Glauert and Horne*, 2005], in which the wave energy is distributed over

195 a range of wave normal angles, we adopt the simpler field-aligned scattering model for our
196 analysis.

Temporal evolution of the electron phase space density was then obtained from a numerical integration of a simplified Fokker-Planck equation in which cross (momentum and pitch-angle) diffusion terms were ignored.

$$\frac{\partial f}{\partial t} = \frac{1}{yT}\frac{\partial}{\partial y}\left(yT\langle D_{yy}\rangle\frac{\partial f}{\partial y}\right) + \frac{1}{p^2}\frac{\partial}{\partial p}\left(p^2\langle D_{pp}\rangle\frac{\partial f}{\partial p}\right) - R_L \tag{4}$$

Here $y = \sin\alpha_{eq}$, R_L is the loss rate, and $T(\alpha_{eq}) = 1.3802 - 0.3198(y + y^{1/2})$. The bounce averaged diffusion coefficient $\langle D_{yy}\rangle$ may be related to the bounce averaged pitch-angle diffusion coefficient $\langle D_{\alpha\alpha}\rangle$ [*Shprits et al.*, 2006b] by

$$\langle D_{yy}\rangle = \left(1 - y^2\right)\langle D_{\alpha\alpha}\rangle. \tag{5}$$

Equation (4) may be simplified further by considering diffusion in pitch-angle and energy separately. The temporal evolution of the pitch-angle distribution can be obtained from

$$\frac{\partial f}{\partial t} = \frac{1}{yT(y)}\frac{\partial}{\partial y}\left(yT(y)\langle D_{yy}\rangle\frac{\partial f}{\partial y}\right) - \frac{f}{\tau_\alpha}, \tag{6}$$

where the electron loss time τ_α is equated to the electron quarter bounce-time inside the loss cone and set to infinity outside the loss cone. Boundary conditions for solution of equation (5) are $\partial f/\partial\alpha = 0$ at $\alpha = 90°$, and f = 0 at $\alpha = 0°$. Exponential decay of the modeled electron distribution function $f(\alpha, p)$ yields the precipitation lifetime $\tau_p(E)$ due to scattering into the atmosphere. Temporal changes in the energy spectrum can then be obtained from the 1-D momentum diffusion equation

$$\frac{\partial f}{\partial t} = \frac{1}{p^2}\frac{\partial}{\partial p}\left(p^2\langle D_{pp}\rangle\frac{\partial f}{\partial p}\right) - \frac{f}{\tau_p(E)} \tag{7}$$

197 where $\langle D_{pp}\rangle$ is also averaged over equatorial pitch-angle.

198 Solutions of equation (7) provide a realistic simulation of the temporal evolution of
199 nearly equatorial particles. CRRES data from orbit 186 was used for our starting condition
200 (diamond symbols in Figure 6). The seed population ($\leq$ 150 keV), provided by inward
201 convection (section 2), was observed to change between orbits 186 and 187 (Figure 1).
202 To account for this, the lower boundary flux in our simulation (at 153 keV) was allowed
203 to gradually increase linearly in time. Flux at the upper boundary (15 MeV) was set to
204 zero. Solutions obtained for the electron phase space density were subsequently converted
205 to differential flux $J = p^2 f$ [*Rossi and Olbert*, 1970] to obtain the evolution of the energy
206 spectrum at L=3.35 (Figure 6a) after 5 hours (dot-dash) and 10 hours (dash). The
207 modeled distribution above 300 keV, ten hours into the simulation, agree remarkably
208 well with CRRES observations on orbit 187 (triangles). Our simulation indicates that
209 local chorus-induced acceleration was a dominant process leading to the enhancement
210 in energetic electron flux in the region normally identified with the slot during the early
211 recovery phase of the October, 1990 storm. The model results yield little change in the flux
212 of MeV electrons, due to the much smaller energy diffusion rates at higher energies (Figure
213 5). Corresponding simulation at L = 3.05 (Figure 6b) indicate that wave acceleration
214 alone, based on the local CRRES measurements, cannot account for flux increases in the
215 inner slot. Average wave amplitudes would have to be considerably higher ($\sim$ 37 pT as
216 indicated by the dotted line) than the local measurements to match CRRES observations.
217 It is more likely that flux enhancements near $L \sim 3$ is due to the combined effect of rapid
218 local acceleration near $L \sim 3.3$ (Figure 6a), followed by modest ($\Delta L \sim 0.3$) inward radial
219 diffusion (e.g. Figure 3), but a 3D diffusion simulation will be needed to confirm this.

5. Statistical Analysis of Slot Region Filling

Although the simulations described above indicate that local wave acceleration provides an effective mechanism to explain energetic electron flux enhancements in the slot region during the early recovery phase of the October 1990 geomagnetic storm, it is important to investigate the viability of this process during other storms. To address this issue we have undertaken a statistical analysis of changes in the energetic electron population, and corresponding changes in the intensity of chorus emissions, and the ratio of f_{pe}/f_{ce} (which controls the rate of energy diffusion) during storm conditions compared to quiet times. We identify storm conditions (when strong convective activity maintains the source population of low-energy electron for chorus excitation) using the magnetic activity index $AE_{max} > 500$ nT over the preceding 3 hours. For quiet times, we adopt $AE_{max} < 100$ nT over the preceding 3 hours. Statistical properties of the perpendicular energetic electron flux $J_{\perp}(L, MLT)$ obtained from the MEA instrument over the entire CRRES mission are shown in Figure 7. Under quiet conditions, the presence of the slot between the inner and outer radiation belts becomes readily apparent at energies above 300 keV. The corresponding intensity of chorus emissions and the ratio f_{pe}/f_{ce} are shown in Figure 8. Enhanced chorus emissions are observed in association with low values of the ratio f_{pe}/f_{ce} outside the plasmasphere in the MLT region from 23:00 to 14:00. To emphasize changes during storm conditions, we plot the ratio of the electron flux for $AE_{max} > 500$ nT compared to that for $AE_{max} < 100$ nT in the top two panels of Figure 9. The storm to quiet time ratio of the wave intensity and of f_{pe}/f_{ce} is shown in the lower two panels. During storm conditions the inner zone is essentially unaffected, but there are large increases in energetic electron flux throughout the outer zone and slot region. The

dawn-dusk asymmetry in 153 keV electron flux is probably due to the influence of the enhanced storm-time convection electric field, but azimuthal gradient drifting removes such effects at 340 keV. The largest storm-time to quiet-time ratio at 340 keV is found within the slot region $L \sim 3$. During storm conditions, the intensity of whistler mode chorus emissions is dramatically enhanced throughout the region exterior to the storm-time plasmapause over an MLT range between 2300-1400. The dawn-side plasmapause is also compressed to L values $\sim$ between 2 and 3, leading to a pronounced decrease in the ratio f_{pe}/f_{ce} in the region normally identified with the quiet-time slot. The combination of low density and high wave intensity provide the requisite conditions for local wave acceleration.

6. Discussion

The process described in section 4, for local wave acceleration of energetic electrons ($>$ 150 keV) in the region just outside the storm-time plasmapause ($L \geq 3$), should also be effective for enhancing the energetic electron flux in the slot region in the early recovery phase of other geomagnetic storms (section 5). Statistical analysis of the properties of chorus emissions indicates the presence of enhanced waves throughout the region exterior to the plasmapause [*Meredith et al.*, 2001, 2003a] in association with sustained convective injection [*Meredith et al.*, 2002b]. The energy diffusion rate (Figure 5) and hence the time-scale for local acceleration is strongly dependent on plasma density and wave properties, and on the energy of resonant electrons. At energies exceeding an MeV, typical acceleration times normally exceed several days [*Horne et al.*, 2005a]. With the cessation of the strong convective injection, associated with the development of the ion ring current during the storm main phase, the boundary of convective injection moves to

higher L, and the plasmapause moves outwards. Enhancement of plasma density near $L \sim 3$ in the recovery phase of moderate geomagnetic storms effectively terminates the wave acceleration process before electrons can be accelerated to energies above 1 MeV. The wave acceleration process can still continue to operate at higher L (in the heart of the outer radiation zone), as long as chorus is excited by sustained substorm injection, as observed during the extended recovery of the October 1990 storm.

During more extreme magnetic storms, both radial diffusion and local wave acceleration can contribute to relativistic electron flux enhancements in the slot region. *Loto'aniu et al.* [2006] have evaluated the rate of radial diffusion by intense ULF waves on October 29, 2003 at the onset of the Halloween storm, and shown that drift resonant acceleration can occur in the slot region near $L \sim 2$ over a time-scale of 24 hours. However, the most intense electron acceleration during the Halloween storm occurred over a period of 3-4 days, well after the cessation of enhanced ULF wave activity [*Horne et al.*, 2005b]. The Halloween storm was unique in that the plasmapause moved well inside $L = 2$ and remained at low L for several days, allowing chorus wave acceleration to continue to accelerate electrons to energies above 3 MeV, producing a new radiation belt peaked at $L = 2.5$ [*Horne et al.*, 2005b; *Shprits et al.*, 2006a]. Local wave acceleration could also account for the delayed injection of > 2 MeV electrons into the slot region in the extended recovery phase of more intense geomagnetic storms with $Dst_{min} <$ -130 nT [*Zheng et al.*, 2006]. However, over the typical three day acceleration period between Dst_{min} and observed flux peaks in the slot region, one cannot discount the contribution of radial diffusion to the injection process. The wave intensities observed on CRRES during the October 1990 storm (Figure 4) were relatively modest. Stronger chorus intensities ($\geq$ 100 pT), together with enhanced

radial diffusion, could possibly account for the rapid (on time scales $\sim$ hours) injection of relativistic electrons into the slot region during major geomagnetic storms [*Nagai et al.*, 2006]. However, 3D modeling will be needed to clarify the relative importance of the two acceleration processes during such intense events.

The wave acceleration process described above indicates that the temporal history of the location of the plasmapause and the duration of enhanced convective activity (and resulting wave excitation), both of which are controlled by solar wind variability, may determine why some storms are effective electron accelerators, while others are not [*Reeves et al.*, 2003]. Losses also play a controlling role, particularly during the main phase of a storm, when the rate of precipitation loss can exceed the rate of acceleration. Although chorus emissions cause microburst precipiation [*O'Brien et al.*, 2004; *Thorne et al.*, 2005b], the net rate of loss is smaller than the rate of local acceleration for relativistic energies [*Horne et al.*, 2005a]. However, electromagnetic ion cyclotron waves, excited by the injection of ring current ions, can cause rapid precipitation loss of electrons above $\sim$ 500 keV on time-scales of a few hours [*Thorne and Kennel*, 1971; *Lyons and Thorne*, 1972; *Albert*, 2003; *Summers and Thorne*, 2003; *Meredith et al.*, 2003b; *Bortnik et al.*, 2006]. The presence of EMIC waves, either near the plasmapause or within dayside plumes, contributes to the inability of MeV electrons to be injected into the slot region during normal storms, in contrast to electrons below $\sim$ 500 keV which are unable to resonate with such waves.

Acknowledgments. This research was funded in part by NASA grant NNG04GN44G and NSF GEM grants ATM-0402615 and ATM-0603191. The authors thank R. Anderson for use of CRRES wave data and S. Liu for assistance with Figure 2.

References

Abel, B., and R. M. Thorne (1998a), Electron scattering loss in Earth's inner magnetosphere 1. Dominant physical processes, *J. Geophys. Res., 103*, 2385.

Abel, B., and R. M. Thorne (1998b), Electron scattering and loss in Earth's inner magnetosphere 2. Sensitivity to model parameters, *J. Geophys. Res., 103*, 2397.

Albert, J. M. (2003), Evaluation of quasi-linear diffusion coeffi-cients for EMIC waves in a multi-species plasma, *J. Geophys. Res., 108*(A6), 1249, doi:10.1029/2002JA009792.

Bortnik, J., R. M. Thorne, T. P. OBrien, J. C. Green, R. J. Strangeway, Y. Y. Shprits, and D. N. Baker (2006), Observation of two distinct, rapid loss mechanisms during the 20 November 2003 radiation belt dropout event, *J. Geophys. Res., 111*, A12216, doi: 10.1029/2006JA011802.

Bortnik, J., R. M. Thorne, and N. P. Meredith (2007), Modeling the propagation characteristics of chorus using CRRES suprathermal fluxes, *J. Geophys. Res.*, submitted.

Brautigam, D. H. and J. M. Albert (2000), Radial diffusion analysis of outer radiation belt electrons during the October 9, 1990, magnetic storm, *J. Geophys. Res., 105*, 291.

Carpenter, D., L, and R. R. Anderson (1992), An ISSE/whistler model of equatorial electron density in the magnetosphere, *J. Geophys. Res., 97*, 1097.

Daglis, I. A., R. M. Thorne, W. Baumjohan, and S. Levi (1999), The terrestrial ring current: origin, formation, and decay, *Rev. Geophys., 37*, (4), 407.

Elkington, S. R., M. K. Hudson, and A. A. Chan (2003), Resonant acceleration and diffusion of outer zone electrons in an asymmetric geomagnetic field, *J. Geophys. Res., 108*(A3), 1116, doi:10.1029/2001JA009202.

Glauert, S. A., and R. B. Horne (2005), Calculation of pitch angle and energy diffusion coefficients with the PADIE code, *J. Geophys. Res., 110*, A04206, doi:10.1029/2004JA010851.

Goldstein, J., B. R. Sandel, W. T. Forrester, M. F. Thomsen, and M. R. Hairston (2005), Global plasmaphere evolution 22-23 April 2001, *J. Geophys. Res., 110*, A12218, doi:10.1029/2004JA011282.

Green, J. C., and M. G. Kivelson (2004), Relativistic electrons in the outer radiation belt: Differentiating between acceleration mechanisms, *J. Geophys. Res., 109*, A03213, doi:10.1029/2003JA010153.

Horne, R. B., and R. M. Thorne (1998), Potential waves for relativistic electron scattering and stochastic acceleration during magnetic storms, *Geophys. Res. Lett., 25*, 3011.

Horne, R. B., and R. M. Thorne (2003), Relativistic electron acceleration and precipitation during resonant interactions with whistler-mode chorus, *Geophys. Res. Lett., 30*(10), 1527, doi:10.1029/2003GL016973.

Horne, R. B., S. A. Glauert, and R. M. Thorne (2003a), Resonant diffusion of radiation belt electrons by whistler-mode chorus, *Geophys. Res. Lett., 30*(9), 1493, doi:10.1029/2003GL016963.

Horne R. B., N. P. Meredith, R. M. Thorne, D. Heynderickx, R. H. A. Iles, and R. R. Anderson (2003b), Evolution of energetic electron pitch angle distributions during storm time electron acceleration to megaelectronvolt energies, *J. Geophys. Res., 108* (A1), 1016, doi:10.1029/2001JA009165.

Horne,R. B., R. M. Thorne, N. P. Meredith, and R. R. Anderson (2003c), Diffuse auroral electron scattering by electron cyclotron harmonic and whistler mode waves during an

isolated substorm, *J. Geophys. Res., 108*(A7), 1290, doi:10.1029/2002JA009736.

Horne, R. B., R. M. Thorne, S. A. Glauert, J. M. Albert, N. P. Meredith, and R. R. Anderson (2005a), Timescale for radiation belt electron acceleration by whistler mode chorus waves, *J. Geophys. Res., 110*, A03225, doi:10.1029/2004JA010811.

Horne, R. B., R. M. Thorne, Y. Y. Shprits, N. P. Meredith, S. A. Glauert, A. J. Smith, S. G. Kanekal, D. N. Baker, M. J. Engebretson, J. L. Posch, M. Spasojevic, U. S. Inan, J. S. Pickett, and P. M. E. Decreau (2005b), Wave acceleration of electrons in the Van Allen radiation belts, *Nature*, *437*, doi:10.1038/nature03939.

Iles R. H. A., N. P. Meredith, A. N. Fazakerley, R. B. Horne (2006), Phase space density analysis of the outer radiation belt energetic electron dynamics, *J. Geophys. Res., 111*, A03204, doi:10.1029/2005JA011206.

Kennel, C. F., and H. E. Petschek (1966), Limit on stably trapped particle fluxes, *J. Geophys. Res., 71*, 1.

Kim, H. J., and A. A. Chan (1997), Fully adiabatic changes in storm time relativistic electron flux, *J. Geophys. Res., 102*, 22,107.

Liu, S., M. W. Chen, L. R. Lyons, H. Korth, J. M. Albert, J. L. Roeder, P. C. Anderson, and M. F. Thomsen (2003), Contribution of convective transport to stormtime ring current electron injection, *J. Geophys. Res., 108*(A10), 1372, doi:10.1029/2003JA010004.

Loto'aniu, I. R. Mann, L. G. Ozeke, A. A. Chan, Z. C. Dent, and D. K. Milling (2006), Radial diffusion of relativistic electrons into the radiation belt slot region during the 2003 Halloween geomagnetic storms, *J. Geophys. Res., 111*, A04218, doi:10.1029/2005JA011355.

Lyons, L. R., and R. M. Thorne (1972), Parasitic pitch angle diffusion of radiation belt particles by ion cyclotron waves, *J. Geophys. Res., 77*, 5608.

Lyons, L. R., and R. M. Thorne (1973), Equilibrium structure of radiation belt electrons, *J. Geophys. Res., 78*, 2142.

Mathie, R. A., and I. R. Mann (2000), A correlation between extended intervals of ULF wave power and storm-time geosynchronous relativistic electron flux enhancements, *Geophys. Res. Lett., 27*, 3261.

Meredith, N. P., R. B. Horne, R. R. Anderson (2001), Substorm dependence of chorus amplitudes: Implications for the acceleration of electrons to relativistic energies, *J. Geophys. Res., 106*(A7), 13165, doi:10.1029/2000JA900156.

Meredith, N. P., R. B. Horne, R. H. A. Iles, R. M. Thorne, R. R. Anderson, and D. Heynderickx (2002a), Outer zone relativistic electron acceleration associated with substorm enhanced whistler mode chorus, *J. Geophys. Res., 107*, 10.1029/2001JA900146.

Meredith, N. P., R. B. Horne, D. Summers, R. M. Thorne, R. H. A. Iles, D. Heynderickx and R. R. Anderson (2002b), Evidence for acceleration of outer zone electrons to relativistic energies by whistler mode chorus, *Ann. Geophys., 20*, 967.

Meredith, N. P., R. B. Horne, R. M. Thorne, and R. R. Anderson (2003a), Favored regions for chorus-driven electron acceleration to relativistic energies in the Earths outer radiation belt, *Geophys. Res. Lett., 30*, (16), 1871, doi:10.1029/2003GL017698.

Meredith N. P., R. M. Thorne, R. B. Horne, D. Summers, B. J. Fraser, R. R. Anderson (2003b), Statistical analysis of relativistic electron energies for cyclotron resonance with EMIC waves observed on CRRES, *J. Geophys. Res., 108*(A6), 1250, doi:10.1029/2002JA009700.

Nagai, T., A. S. Yakimatu, A. Matsuoka, K. T. Asai, J. C. Green, T. G. Onsager, and H. J. Singer (2006), Timescales of relativistic electron enhancements in the slot region, *J. Geophys. Res., 111*, A11205, doi:10.1029/2006JA011837.

O'Brien T. P., M. D. Looper, and J. B. Blake (2004), Quantification of relativistic electron microbursts losses during the GEM storms, *Geophys. Res. Lett., 31*, L04802, doi:10.1029/2003GL018621.

Reeves, G. D., K. L. McAdams, R. H. W. Friedel, and T. P. O'Brien (2003), Acceleration and loss of relativistic electrons during geomagnetic storms, *Geophys. Res. Lett., 30*, doi10.1029/2002GL016513.

Rossi, B., and S. Olbert (1970), *Introduction to the Physics of Space*, McGraw Hill, New York.

Schulz, M., and L. Lanzerotti (1974), *Particle Diffusion in the Radiation Belts*, Springer, New York.

Sheeley, B. W., M. B. Moldwin, H. K. Rassoul, and R. R. Anderson (2001), An empirical plasmasphere and trough density model: CRRES observations, *J. Geophys. Res., 106*, 25631.

Shprits Y. Y., and R. M. Thorne (2004), Time dependent radial diffusion modeling of relativistic electrons with realistic loss rates, *Geophys. Res. Lett., 31*, L08805, doi:10.1029/2004GL019591.

Shprits, Y. Y., R. M. Thorne, G. D. Reeves, and R. Friedel (2005), Radial diffusion modeling with empirical lifetimes: comparison with CRRES observations, *Ann. Geophys., 23*, 1467.

Shprits, Y. Y., R. M. Thorne, R. B. Horne, M. Cartwright, C. T. Russell, D. Baker, and S. G. Kanekal (2006a), Acceleration mechanism responsible for the formation of the new radiation belt during the 2003 Halloween solar storm, *Geophys. Res. Lett., 33*, L05104, doi:10.1029/2005GL024256.

Shprits, Y. Y., R. M. Thorne, R. B. Horne, and D. Summers (2006b), Bounce-averaged diffusion coefficients for field-aligned chorus waves, *J. Geophys. Res., 111*, A10225, doi:10.1029/2006JA011725.

Stern, D. P. (1975), The motion of a proton in the equatorial magnetosphere, *J. Geophys. Res., 80*, 595.

Summers, D., R. M. Thorne, and F. Xiao (1998), Relativistic theory of wave-particle resonant diffusion with application to electron acceleration in the magnetosphere, *J. Geophys. Res., 103*, 20,487.

Summers, D., C. Ma, N. P. Meredith, R. B. Horne, R. M. Thorne, D. Heynderickx, and R. R. Anderson (2002), Model of the energization of outer-zone electrons by whistler-mode chorus during the October 9, 1990 geomagnetic storm, *Geophys. Res. Lett., 29*, 10.1029/2002GL016039.

Summers, D., and R. M. Thorne (2003), Relativistic electron pitch-angle scattering by electromagnetic ion cyclotron waves during geomagnetic storms, *J. Geophys. Res., 108*(A4), 1143, doi:10.1029/2002JA009489.

Thorne, R. M. (1982), Injection and loss mechanisms for energetic ions in the inner Jovian magnetosphere, *J. Geophys. Res., 87*, 8105.

Thorne, R. M. and C. F. Kennel (1971), Relativistic electron precipitation during magnetic storm main phase, *J. Geophys. Res., 76*, 4446.

443 Thorne, R. M., R. B. Horne, S. A. Glauert, N. P. Meredith, Y. Y. Shprits, D, Summers,
444 and R. R. Anderson (2005a), The influence of wave-particle interactions on relativistic
445 electron dynamics during storms, in *Inner Magnetosphere Interactions: New Perspec-*
446 *tives from Imaging, Geophys. Monogr. Ser.*, vol. 159, edited by James L. Burch, Michael
447 Schulz, and Harlan Spence, pp 101-112, AGU, Washington, D. C.

448 Thorne, R. M., T. P. O'Brien, Y. Y. Shprits, D. Summers, and R. B. Horne (2005b),
449 Timescale for MeV electron microbursts loss during storms, *J. Geophys. Res., 110*,
450 A09202, doi:10.1029/2004JA010882.

451 Volland, H. (1973), A semi empirical model of large-scale magnetospheric electric fields,
452 *J. Geophys. Res., 78*, 171.

453 Zheng, Y., A. T. Y. Lui, X. Li, and M. C. Fok (2006), Characteristics of 2-6 MeV
454 electrons in the slot region and inner radiation belt, *J. Geophys. Res., 111*, A10204,
455 doi:10.1029/2006JA011748.

Figure 1. (top) Variation of the intensity of whistler-mode chorus, Dst, AE, and Kp during the October, 1990 storm. The white line is an empirical estimate of the location of the plasmapause [*Carpenter and Anderson*, 1992]. (bottom) Radial profiles of energetic electron flux observed by the MEA instrument at selected orbits of CRRES, indicated by the black vertical bars in the top panel.

Figure 2. Drift paths for energetic electrons of prescribed magnetic moment due to the combined effect of gradient drifting and convection for both quiet ($\Delta\Phi = 25$ kV) and storm ($\Delta\Phi = 200$ kV) conditions.

Figure 3. Simulation of radial diffusive injection of 340 keV electrons into the slot region after 5 hours (dot-dash) and 10 hours (dash) during the early recovery phase of the October, 1990 storm.

Figure 4. (top) The power spectral intensity of whistler-mode chorus emissions observed between $3.05 \leq L \leq 3.25$ on CRRES (orbit 186 inbound) during the early recovery phase of the October, 1990 storm. Modeled Gaussian fits (red) to the average spectra (green) are also shown, together with the fitted wave amplitude B_w, peak normalized wave frequency x_o, and normalized bandwidth dx. (middle) Observed chorus intensity between $3.35 \leq L \leq 3.55$. (bottom) Average intensity of chorus as a function of L during orbit 186, indicating the presence of strong emissions at $L > 2.7$.

Figure 5. Modeled pitch-angle and momentum diffusion coefficients for electron interaction with chorus emissions at $L \sim 3.35$.

Figure 6. (top) Simulation of the hardening of the energetic electron spectrum at $L = 3.35$ due to local acceleration by chorus emissions in the early recovery phase of the October, 1990 storm. (bottom) Similar simulation at $L = 3.05$.

Figure 7. Statistical properties of energetic electron flux observed by the MEA instrument over the entire CRRES mission for three different levels of geomagnetic activity.

Figure 8. Statistical properties of the intensity of lower band chorus emissions and the ratio f_{pe}/f_{ce} over the entire CRRES mission for three different levels of geomagnetic activity.

Figure 9. Ratios of the change in energetic electron flux (top panels) and chorus intensity and f_{pe}/f_{ce} (bottom panels) during storm conditions ($AE_{max} > 500$ nT) compared to quiet times ($AE_{max} < 100$ nT).

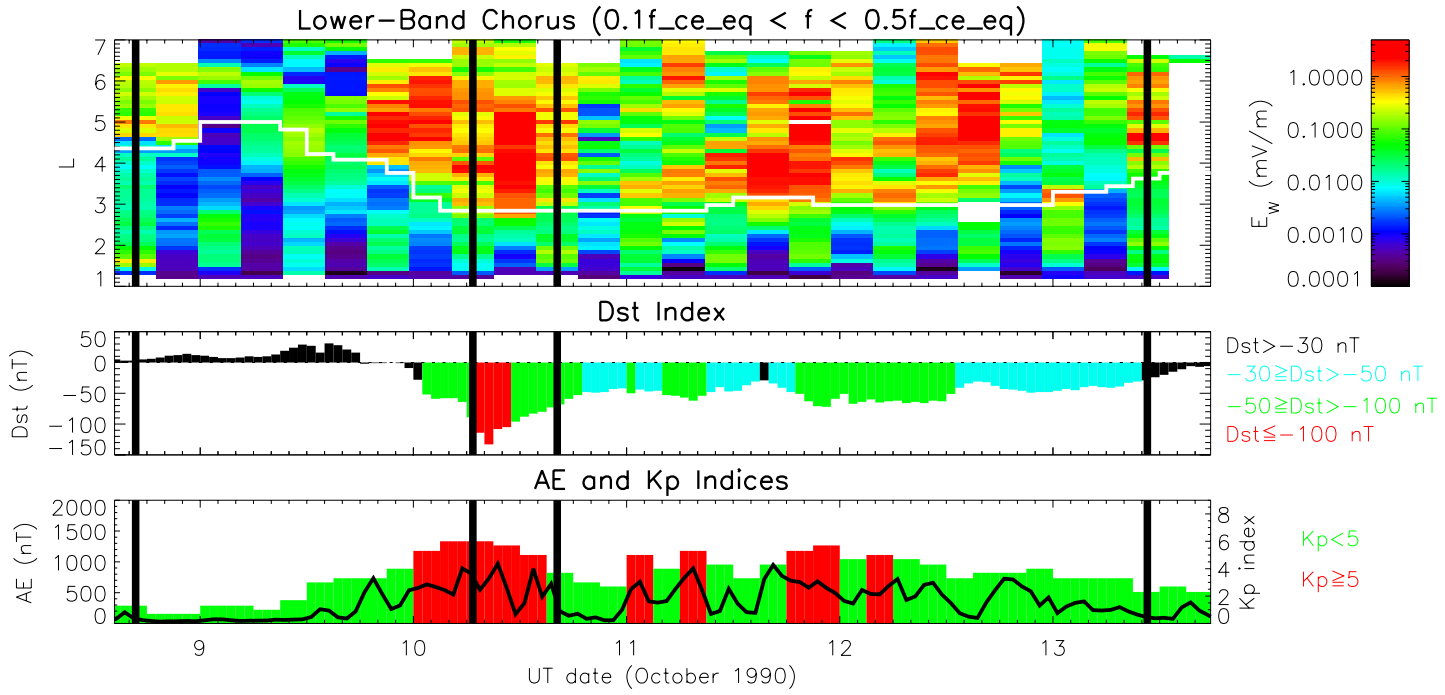
Lower−Band Chorus (0.1f_ce_eq < f < 0.5f_ce_eq)
L
E_w (mV/m)
1.0000
0.1000
0.0100
0.0010
0.0001
Dst Index
Dst (nT)
Dst>−30 nT
−30≥Dst>−50 nT
−50≥Dst>−100 nT
Dst≤−100 nT
AE and Kp Indices
AE (nT)
Kp index
Kp<5
Kp≥5
UT date (October 1990)

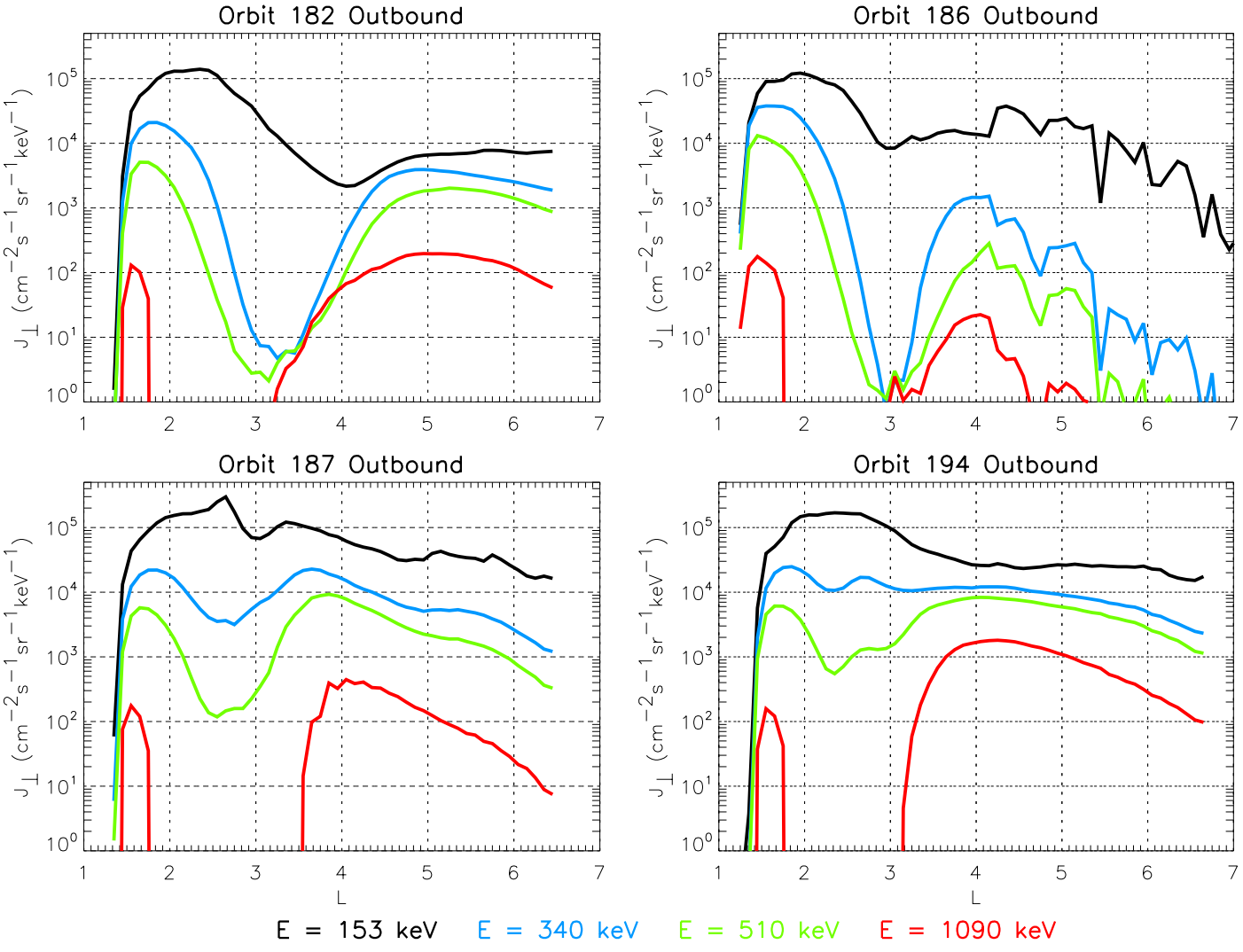
Orbit 182 Outbound
Orbit 186 Outbound
Orbit 187 Outbound
Orbit 194 Outbound
$J_\perp$ (cm^{-2}s^{-1}sr^{-1}keV^{-1})
L
E = 153 keV
E = 340 keV
E = 510 keV
E = 1090 keV

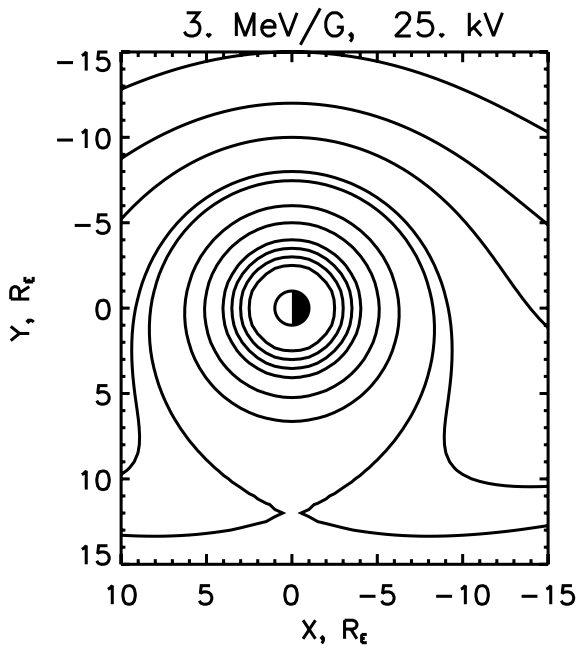
3. MeV/G, 25. kV
−15
−10
−5
0
5
10
15
Y, R$_E$
10
5
0
−5
−10
−15
X, R$_E$

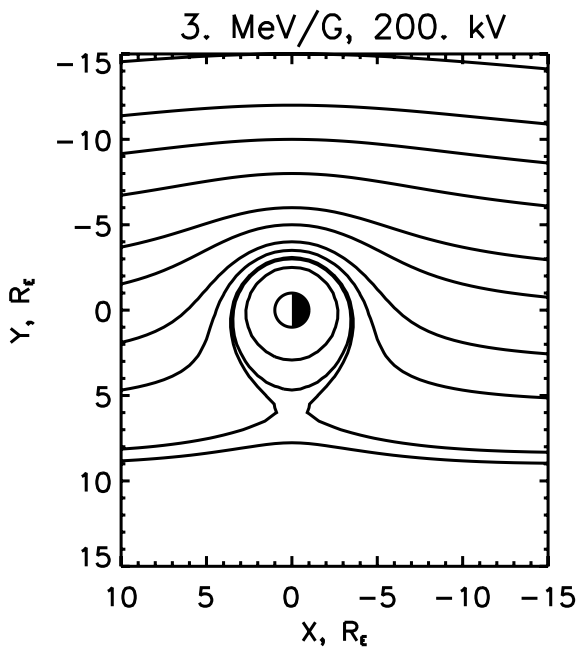
3. MeV/G, 200. kV
−15
−10
−5
0
5
10
15
Y, R$_E$
10
5
0
−5
−10
−15
X, R$_E$

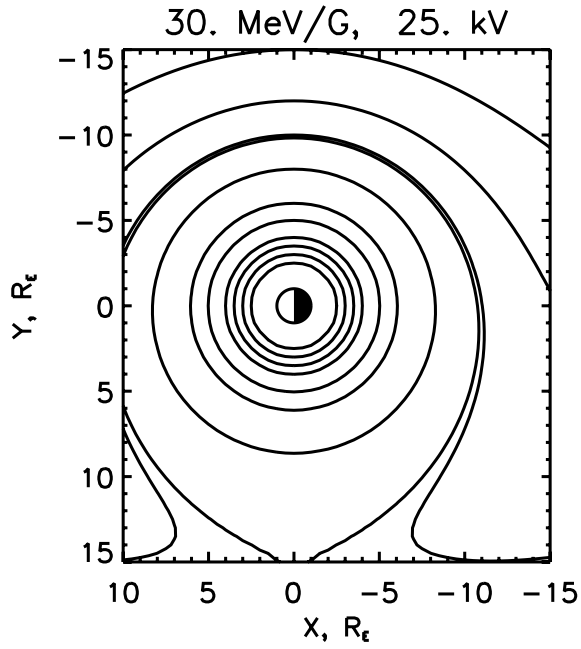
30. MeV/G, 25. kV
−15
−10
−5
0
5
10
15
Y, R$_E$
10
5
0
−5
−10
−15
X, R$_E$

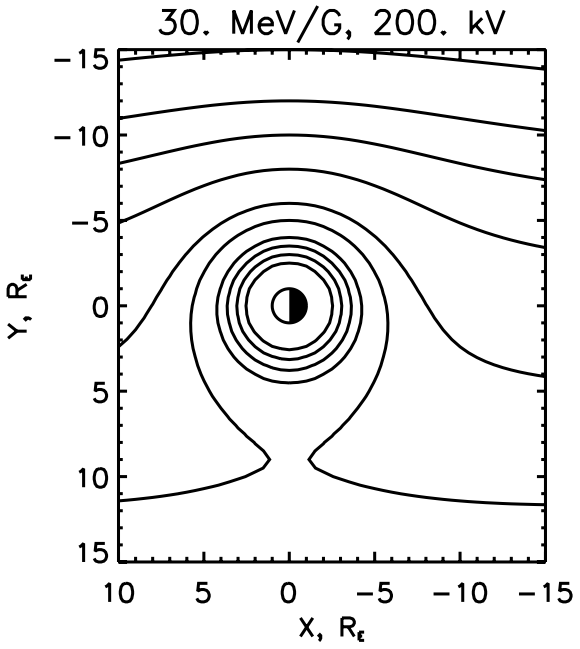
30. MeV/G, 200. kV
−15
−10
−5
0
5
10
15
Y, R$_E$
10
5
0
−5
−10
−15
X, R$_E$

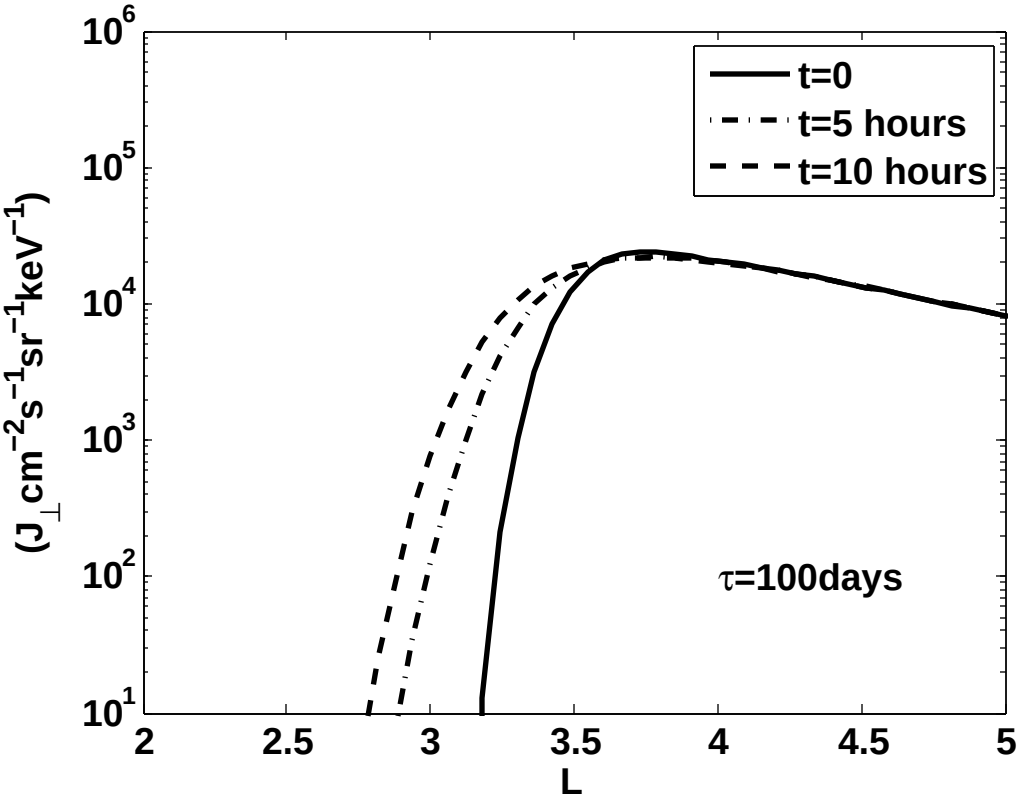
t=0
t=5 hours
t=10 hours
τ=100days
10^6
10^5
10^4
10^3
10^2
10^1
$(J_\perp cm^{-2}s^{-1}sr^{-1}keV^{-1})$
2
2.5
3
3.5
4
4.5
5
L

Orbit 186

Spectral intensity versus relative frequency

L=3.05 MLT=09:46 MLAT=21.3° fce_eq=31.7 kHz

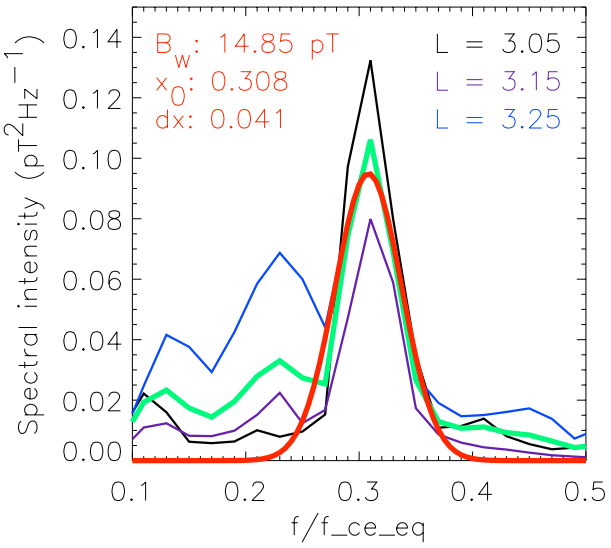

Spectral intensity versus relative frequency

L=3.35 MLT=09:26 MLAT=22.4° fce_eq=23.8 kHz

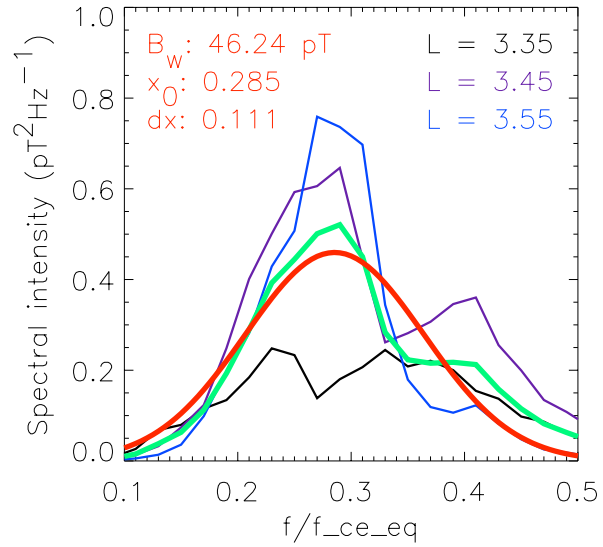

Lower band chorus intensity versus L shell

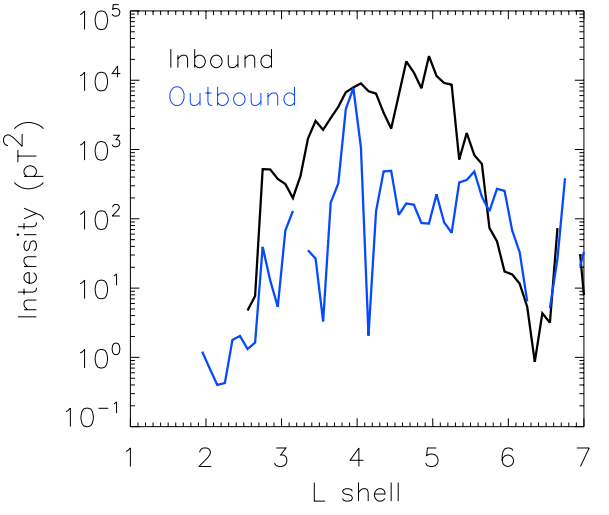

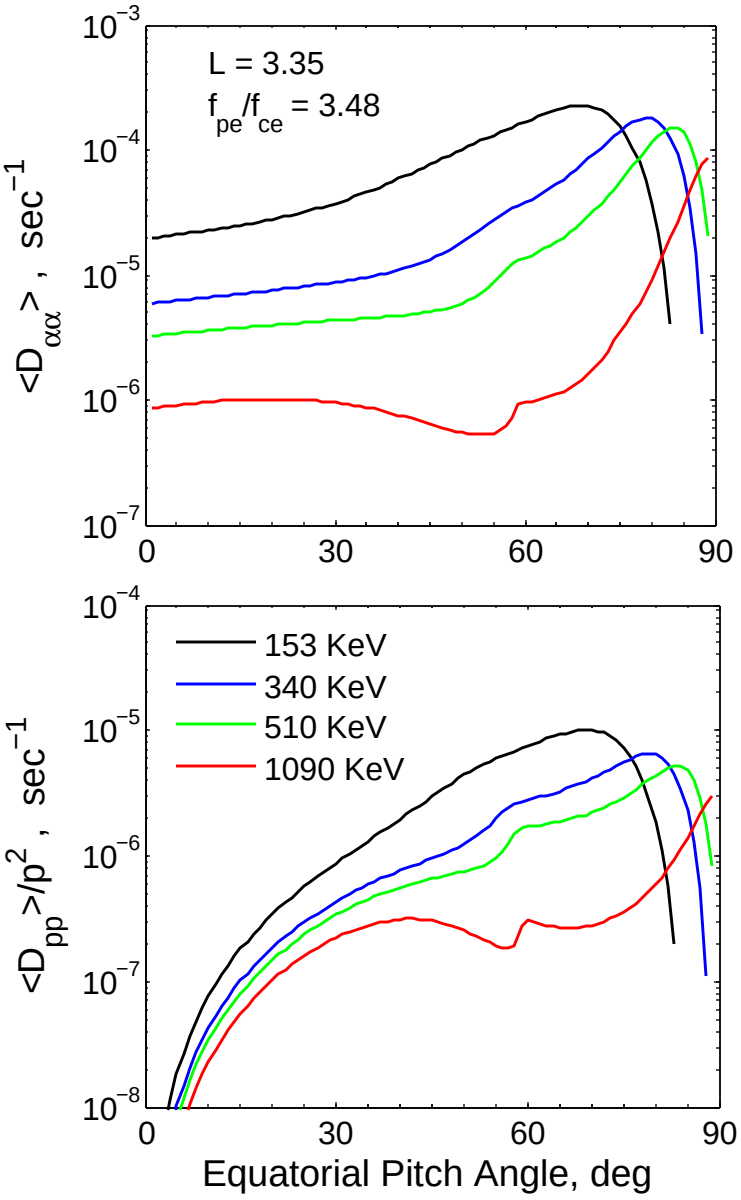
L = 3.35
f_pe/f_ce = 3.48
<D_αα>, sec^-1
<D_pp>/p^2, sec^-1
153 KeV
340 KeV
510 KeV
1090 KeV
Equatorial Pitch Angle, deg

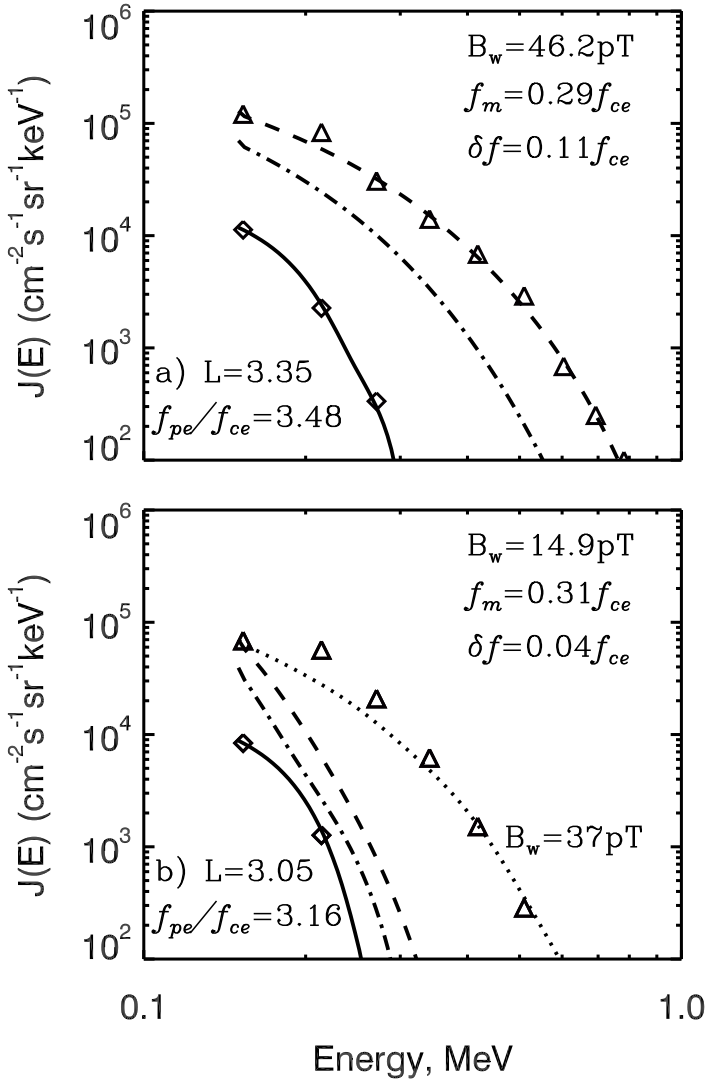
B_w=46.2pT
f_m=0.29f_{ce}
δf=0.11f_{ce}
a) L=3.35
f_{pe}/f_{ce}=3.48
B_w=14.9pT
f_m=0.31f_{ce}
δf=0.04f_{ce}
B_w=37pT
b) L=3.05
f_{pe}/f_{ce}=3.16
J(E) (cm^{-2}s^{-1}sr^{-1}keV^{-1})
10^2
10^3
10^4
10^5
10^6
0.1
1.0
Energy, MeV

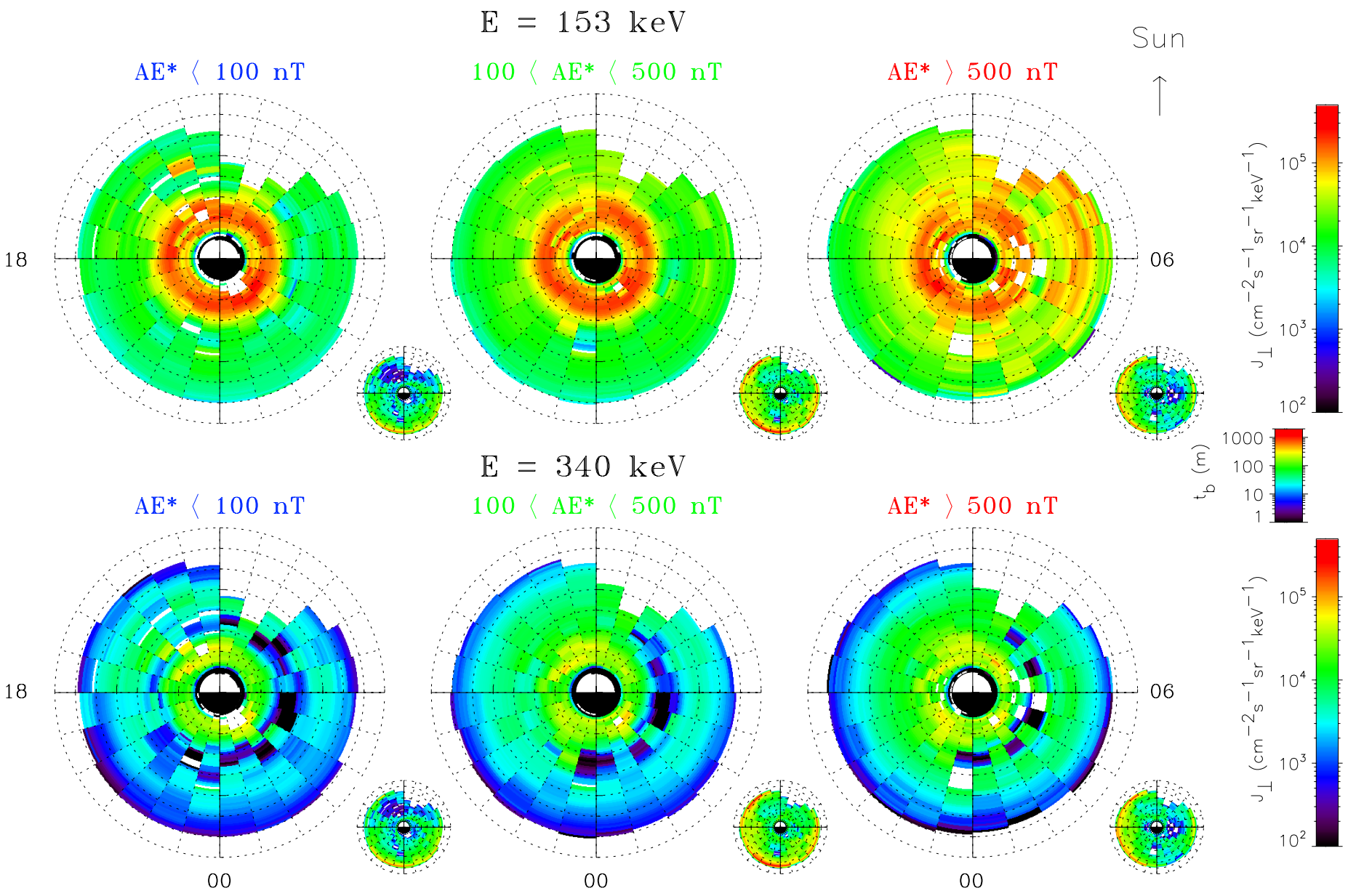
E = 153 keV
AE* ⟨ 100 nT
100 ⟨ AE* ⟨ 500 nT
AE* ⟩ 500 nT
Sun
18
06
00
E = 340 keV
AE* ⟨ 100 nT
100 ⟨ AE* ⟨ 500 nT
AE* ⟩ 500 nT
18
06
00
$J_\perp$ (cm^{-2}s^{-1}sr^{-1}keV^{-1})
10^5
10^4
10^3
10^2
t_b (m)
1000
100
10
1
$J_\perp$ (cm^{-2}s^{-1}sr^{-1}keV^{-1})
10^5
10^4
10^3
10^2

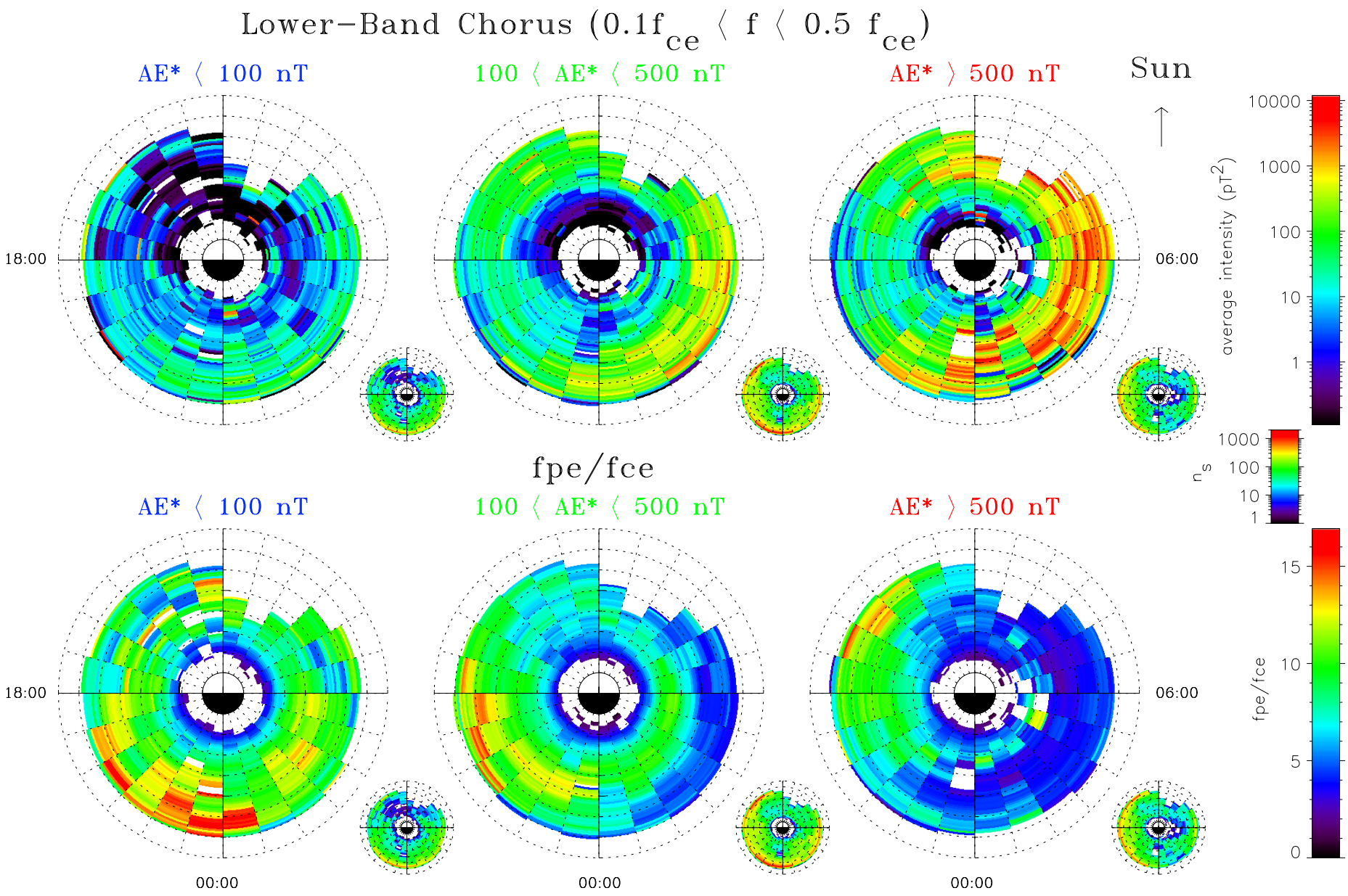
Lower−Band Chorus (0.1f ce ⟨ f ⟨ 0.5 f ce)
AE* ⟨ 100 nT
100 ⟨ AE* ⟨ 500 nT
AE* ⟩ 500 nT
Sun
18:00
06:00
00:00
average intensity (pT2)
10000
1000
100
10
1
fpe/fce
ns
15
5
0

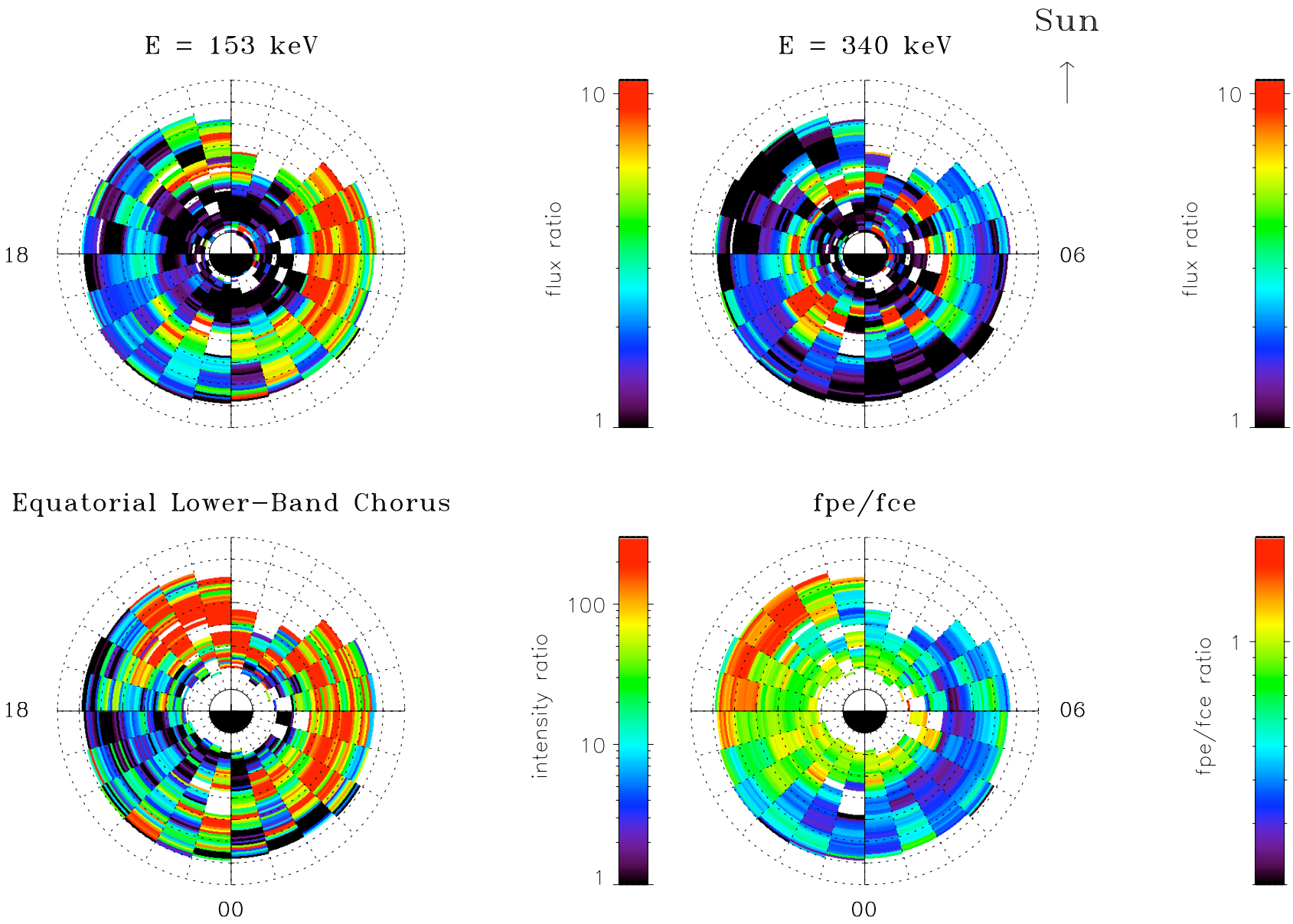
E = 153 keV
E = 340 keV
Sun
18
06
00
10
1
flux ratio
Equatorial Lower-Band Chorus
fpe/fce
100
intensity ratio
fpe/fce ratio